PCCP

Accepted Manuscript

This is an *Accepted Manuscript*, which has been through the Royal Society of Chemistry peer review process and has been accepted for publication.

Accepted Manuscripts are published online shortly after acceptance, before technical editing, formatting and proof reading. Using this free service, authors can make their results available to the community, in citable form, before we publish the edited article. We will replace this *Accepted Manuscript* with the edited and formatted *Advance Article* as soon as it is available.

You can find more information about *Accepted Manuscripts* in the **Information for Authors**.

Please note that technical editing may introduce minor changes to the text and/or graphics, which may alter content. The journal's standard **Terms & Conditions** and the **Ethical guidelines** still apply. In no event shall the Royal Society of Chemistry be held responsible for any errors or omissions in this *Accepted Manuscript* or any consequences arising from the use of any information it contains.

ARTICLE TYPE

Synthesis and luminescence resonance energy transfer based on noble metal nanoparticles and NaYF$_4$:Tb^{3+} shell

Yan Song, Guixia Liu*, Jinxian Wang, Xiangting Dong, Wensheng Yu

A core-shell hybrid nanostructure was prepared combining NaYF$_4$ doped with the lanthanide dopants Tb^{3+} as shell layer materials and noble metal nanoparticles (Au, Ag) as cores. For the core-shell system, the luminescence resonance energy transfer (LRET) was demonstrated, in which noble metal nanoparticles as fluorescence quenchers can absorb the emission energy of α-NaYF$_4$:Tb^{3+} donor. The

10 morphology, structure, composition and properties of the as-prepared samples were characterized by X-ray powder diffraction (XRD), transmission electron microscopy (TEM), energy dispersive spectroscopy (EDS), X-ray photoelectron spectroscopy (XPS), UV-Vis absorption and photoluminescence (PL) spectra, respectively. In Au/Ag@NaYF$_4$:Tb^{3+} system, it is observed that the plasmonic absorption bands of gold or silver nanoparticles overlap with the emission bands of $^5D_4 \rightarrow {}^7F_j$ (j= 6,5) transition of the Tb^{3+} ions,

15 and the emission intensity of the $^5D_4 \rightarrow {}^7F_5$ transition is clearly attenuated. The photoluminescence decay curve measurements show that the lifetimes of the $^5D_4 \rightarrow {}^7F_6$ and $^5D_4 \rightarrow {}^7F_5$ transitions of Tb^{3+} are slightly decreased in the presence of gold or silver cores. The quenching efficiency of the gold and silver nanoparticles implies that the efficiency of energy transfer is highly dependent on the extent of spectral overlap in the LRET system.

1 Introduction

20 In recent years, noble metal nanoparticles such as gold, silver and platinum have attracted particular interest and extensive research because of their unique surface plasmon resonance (SPR) property. Noble metal nanoparticles have the ability to sustain

25 oscillation of electrons known as surface plasmon leading to electromagnetic fields confined to the metal surface. In plasmonics, metal nanostructures can serve as antennas to convert light into localized electricfields and significantly alter the electromagnetic field surrounding of the noble metal

30 nanoparticles.[1-3] In particular, gold nanoparticles occur strongly resonance at their plasmon wavelengths in the visible region and the strong plasmon resonance enhances light scattering of metal nanoparticles. The light scattering properties of gold nanoparticles have been utilized recently for biological imaging[4-6].

35 Moreover, the ability of gold nanoparticles to absorb light and convert it to heat is a fascinating property. The efficient conversion from light into heat by these noble metal nanoparticles, particularly of gold, can be allowed due to surface plasmon resonance or energy transfer band. In this case, noble

40 metal nanoparticles may be considered as photothermal therapy in medicine[7, 8]. Simultaneously, it is an emerging field with the potential to have a positive effect on human healthcare[9-11].

In the case of electro-magnetic interaction between nanoparticles and dipole emitters, surface plasmon resonance of

45 noble metal nanoparticles have either beneficial or deleterious effect，which depends on the position of the plasmon resonance peaks and the distance between the emitter and the plasmonic metal nanoparticles surface.[12, 13] It is reported that the plasmon resonance of the noble metal nanoparticles can affect

50 fluorescence quenching or enhancement, which depends on the spacing distance between the lanthanide-based luminescence material and the noble metal nanoparticles.[13-15] Efficient luminescent enhancement can be achieved, when the luminescences nanocrystals move away from the surface of noble

55 metal nanoparticles and keep at some critical distance[15-22]. In contrast, if the luminescent nanoparticles are direct contacted with metal nanoparticles, fluorescent quenching will occur and accompany with the resonance energy transfer[22, 23], which can be explained by luminescence resonance energy transfer(LRET). In

60 LRET system, gold nanoparticles as fluorescence acceptor must absorb energy at the emission wavelengths of the donor.

Previously, there have been a number of reports describing the fabrication of gold nanoparticles with fluorescent dyes or quantum dots in various particular research areas.[13, 24-28] But the

65 inherent limitations of these systems, including high background noise, potential toxicity, and instability, cannot be eliminated by incorporating LRET technology and still restrict their application in the analysis of biological samples. In comparison to organic dyes and quantum dots, lanthanide-doped inorganic systems are a

70 powerful tool for both biological and medical applications due to their photostability and photoflashing, low toxicity, biocompatibility and long luminescence lifetime.[29] Moreover, these lanthanide-based luminescent materials enable prolonged

LRET sensing due to their photostability, low cytotoxicity, good light penetration depth, and minimum photodamage. There have some works of the LRET system based on lanthanide-doped nanoparticles as donor and gold nanoparticles as quencher-like acceptor[30-36]. In various matrixes, $NaYF_4$ nanocrystals have attracted a lot of attention in the last few years as luminescent host matrices for applications mainly in the field of optical labeling.[37]Lanthanide dopant ions, such as Tb^{3+}, show advantages for use as donors for resonance energy transfer studies due to their large stokes shifts and narrow emission lines arising from 4f-4f transitions. Thus, Tb^{3+} ions are selected as dopants base on the particularly important reason. Then, the LRET system is constructed and multifunctional property can be achieved.

In this work, we described the synthesis and characterization of a hybrid core-shell nanostructure of $NaYF_4:Tb^{3+}$ nanoshells and gold or silver nanocores by a facile solution method. In such a LRET system, cubic phase $NaYF_4:Tb^{3+}$ serves as energy donor and noble metal nanoparticles serve as energy acceptor, energy transfer from the luminescent nanoparticles to the noble metal nanoparticles may be occurred. The LRET was studied by the variation of the emission intensity and PL lifetime of Tb^{3+} in the absence and presence of noble metal nanoparticles. It is observed that the noble metal nanoparticles as acceptor have quenching effect on luminescence of $NaYF_4:Tb^{3+}$, and the quenching effect depended on plasmon wavelengths. The hybrid nanostructure will be available used for second modality imaging because of combining $NaYF_4:Tb^{3+}$ luminescent materials and noble metal nanoparticles. Considering the LRET from Tb^{3+} ions to gold or silver, hybrid core-shell nanoparticles perhaps open exciting opportunities in the biomedical fields of imaging, sensing and thermal therapy.

2 Experimental section

Chemicals

Yttrium oxide (Y_2O_3), terbium oxide (Tb_4O_7), ammonium fluoride (NH_4F), sodium citrate, ethylene glycol (EG), Polyvinylpyrrolidone (PVP), nitric acid (HNO_3) and ethanol were purchased from Sinopharm Chemical Reagent Co., Ltd. Silver nitrate ($AgNO_3$) and gold chloride tetrahydrate ($HAuCl_4$), were purchased from Aladdin. Deionized water (DI water) was used as the common solvent unless stated otherwise. All the chemicals in this investigation were used without further purification.

Rare earth nitrate stock solutions were prepared by dissolving the corresponding rare earth oxides in dilute HNO_3 under heating with agitation followed by evaporating the solvent.

Synthesis of Au and Ag nanoparticles

The gold nanoparticles were prepared according to the literature with some modification, as described by Frens and Turkevich[38,39]. In more details, 0.015 mmol of $HAuCl_4$ aqueous solution was diluted with 92 mL DI water to form bright yellow solution. The aqueous solution of $HAuCl_4$ was heated to boil and vigorously stirred by Teflon-coated magnetic bars for 15 minutes. Then the 0.05 mmol sodium citrate solution was rapidly injected into the boiling $HAuCl_4$ aqueous solution under vigorous stirring. After still refluxing for 15 min, the solution was cooled to room temperature and appeared wine red, indicating gold nanoparticles were formed. The synthesized nanoparticles were used in further experiments without washing.

Silver nanoparticles were prepared by following the reported method[17]. Briefly, $AgNO_3$ (100 mg) and PVP (0.5g, K30) were dissolved in 40 ml EG with continuous stirring at room temperature. Subsequently, the solution was heated up to 130 °C at a constant rate of 10 °C/min, and the reaction continued for 1 h at this temperature. When the mixture was cooled to room temperature, the silver was recovered by centrifugation at 8000 rpm for 5 min with a large amount of acetone. The silver nanoparticles were washed with ethanol and DI water, and then dispersed in 5 mL of DI water.

$NaYF_4:Tb^{3+}$ nanoshell encapsulation

The as-prepared gold colloidal solution (30 ml) or silver nanoparticles (2 mg), sodium citrate solution (0.02 mmol), $Y(NO_3)_3$ (0.019 mmol), $Tb(NO_3)_3$ (0.001 mmol) solutions were mixed together at room temperature and stirred for 30 min. Subsequently, 0.24 mmol NH_4F was then introduced dropwise. The mixture was stirred at room temperature for 1 h. The resulting core-shell nanoparticles were collected by centrifugation at 7000 rpm for 5 min , washed at least twice with DI water and ethanol for several times and then dispersed either in ethanol or water for further characterization.

Characterizations

The crystalline nature and phase composition of the as-synthesized products were examined by X-ray powder diffraction (XRD) using a Bruker D8 FOCUS with Cu Kα radiation (λ= 1.54056 Å). The morphology and size of the all samples were characterized by a JEOL JEM-2010 transmission electron microscope (TEM) under a working voltage of 200 kV. The energy-dispersive spectroscopic (EDS) analysis was performed using an Oxford INCA energy system operated at 200 kV. X-ray photoelectron spectrum (XPS) was recorded on a VG ESCALAB MK II electron energy spectrometer with a standard Al Kα source. UV-Vis absorption spectra were obtained using Shimadzu UV-2450 spectrophotometer. The photoluminescence spectra and the decay curve measurements were carried out on F-7000 spectrophotometer at room temperature equipped with a 150 W xenon lamp as the excitation source(PMT voltage: 700 V, slit widths: Ex 2.5 nm and Em 2.5 nm).

3 Results and discussion

3.1 Structure characterization of nanocomposites

Figure 1 shows the X-ray diffraction patterns of the $NaYF_4:Tb^{3+}$ nanocrystals and $Au@NaYF_4:Tb^{3+}$ nanoparticles. It is noted that the diffraction peaks can be readily indexed to the pure cubic phase $NaYF_4$ crystal, the locations and relative intensities of the diffraction peaks coincide well with the standard card (JCPDS card 77-2042) of $NaYF_4$. No other diffraction peaks or impurities are found, indicating that pure α-$NaYF_4$ can be obtained under this condition. From Figure 1(b), it can be seen that besides the characteristic peaks of α-$NaYF_4$ crystals, several diffraction peaks of gold are also found. The peaks of Au correspond well with the standard card (JCPDS card 65-2870) and are indexed to the (111), (200), (220) and (311) planes, indicating the existent of gold and α-$NaYF_4:Tb^{3+}$ in the hybrid nanoparticles.
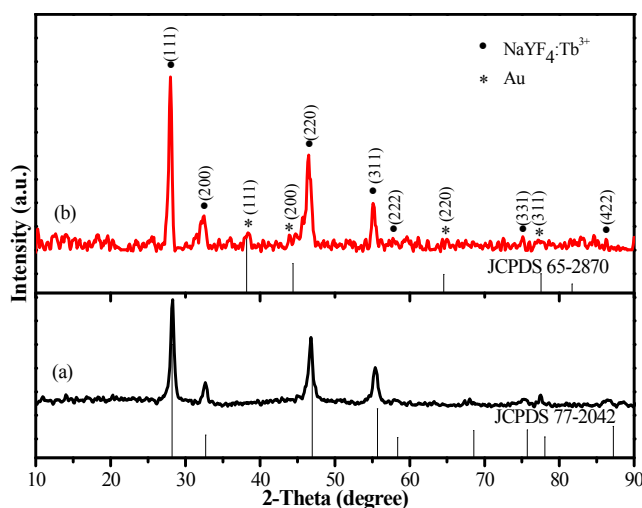
Figure 1. XRD patterns of NaYF$_4$:Tb^{3+} nanoparticles (a) and Au@NaYF$_4$:Tb^{3+} nanoparticles (b). The standard card of α-NaYF$_4$ and Au were given as reference.
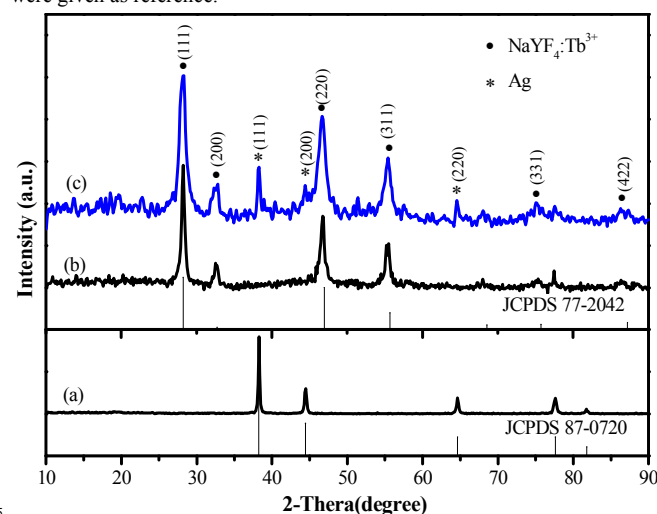
Figure 2. XRD patterns of Ag nanoparticles (a), NaYF$_4$:Tb^{3+} nanocrystals (b) and Ag@NaYF$_4$:Tb^{3+} nanoparticles (c). The standard card of α-NaYF$_4$ and Ag were given as reference.

The XRD pattern of the as-prepared Ag@NaYF$_4$:Tb^{3+} is shown in Figure 2. The strong peaks positioning at 28.2°, 32.7°, 46.9°, 55.7°, 75.7° and 87.2° correspond to the (111), (200), (220), (311), (331) and (422) lattice planes of the standard face-centered cubic phase of NaYF$_4$ (JCPDS card 77-2042), respectively. Compared to NaYF$_4$:Tb^{3+} nanoparticles, there are some additional peaks at 2θ = 38.2°, 44.4°, 64.6° in Ag@NaYF$_4$:Tb^{3+} nanoparticles, which agree well with the JCPDS card 87-0720 of silver. The XRD pattern confirms the presence of both Ag and NaYF$_4$:Tb^{3+} crystals in the formed Ag@NaYF$_4$:Tb^{3+} structure. Hence, the synthesis method is an effective method for fabricating hybrid nanoparticles.

3.2 Morphology and composition characterization of the nanocomposites

Figure 3a shows a typical TEM image of Au nanoparticles. It can be seen that the Au nanoparticles are close to spherical in shape and appear to be relatively uniform in size with an average diameter of about 12-20 nm. From the image shown in Figure 3b, we can see that the gold nanoparticles are surrounded by the NaYF$_4$:Tb^{3+} nanoshell layer with the thickness of 5-10 nm, which is clear in the inset image of Figure 3b. Moreover, EDS analysis (Figure 3c) of Au@NaYF$_4$:Tb^{3+} nanoparticles further reveals their elemental composition. There are C, Y, Na, F, Tb and Au elements in the sample of Au@NaYF$_4$:Tb^{3+} samples. Among those elements, Y, Na and F in the EDS spectrum confirm the formation of the NaYF$_4$:Tb^{3+} nanocrystals. In addition to these elements, the spectrum also includes the peaks of Au, which indicates the existence of Au in the nanocomposites. The same scheme is used for Ag as the core, which leads to the formation of smooth Ag@NaYF$_4$:Tb^{3+} nanoparticles. From the SEM image (Figure 3d), it can be seen that the Ag@NaYF$_4$:Tb^{3+} nanoparticles are almost spherical morphologies and have good uniformity in size. The obtained particle size histogram shows that the average diameter of the Ag@NaYF$_4$:Tb^{3+} nanoparticles is 116 nm. As revealed by TEM image (Figure 3e), the Ag@NaYF$_4$:Tb^{3+} composites have a mean diameter of about 110 nm, which is consistent with the SEM results, and the NaYF$_4$:Tb^{3+} nanoshell layer thickness is about 10 nm. The EDS (Figure 3f) of Ag@NaYF$_4$:Tb^{3+} nanoparticles also reveals their elements of the core-shell nanocomposites. Ag, C, Na, F, Y and Tb can all be easily found in the EDS graph. The signals resulted from TEM and EDS of the product confirm the formation of Ag@NaYF$_4$:Tb^{3+} nanoparticles.
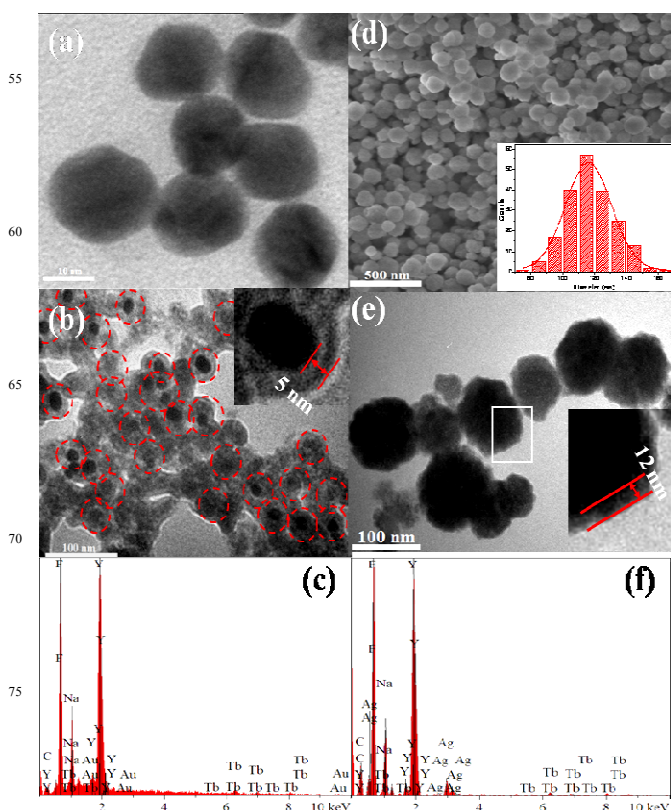
Figure 3. TEM images of Au nanoparticles (a), Au@NaYF$_4$:Tb^{3+} nanoparticles (b) (Inset is the enlarged TEM image corresponded to the Au@NaYF$_4$:Tb^{3+} nanoparticles) and Ag@NaYF$_4$:Tb^{3+} nanoparticles (e) (Inset is the enlarged TEM image), SEM image of Ag@NaYF$_4$:Tb^{3+} (d) (Inset is the particle size histogram), EDS of Au@NaYF$_4$:Tb^{3+} nanoparticles (c) and Ag@NaYF$_4$:Tb^{3+} nanoparticles(f).

To further confirm the coating of the $NaYF_4$:Tb^{3+} shells on the Au or Ag cores. The relative surface composition of Au@$NaYF_4$:Tb^{3+} and Ag@$NaYF_4$:Tb^{3+} nanoparticles was analyzed by XPS (Figure 4). The full range surveys of XPS wide spectra of Au@$NaYF_4$:Tb^{3+} (a) and Ag@$NaYF_4$:Tb^{3+} (b) are shown in Figure 4A. In Figure 4A, curve (b) shows the same as curve (a). The XPS spectrum shows the presence of C, O, F, Y and Tb elements and weak peaks of Au or Ag. In the case of Au 4f core magnified level spectrum (Figure 4A. inset i), the Au 4f peaks show a doublet at 83.5 and 87.1 eV corresponding to Au $4f_{7/2}$ and Au $4f_{5/2}$, respectively. It suggests that Au is mainly present in Au^0 state. The peak at 367.7 eV is attributed to the binding energy of Ag (Figure 4A. inset ii). For the restriction of penetrating depth of XPS, the weak Au and Ag peaks indicate that the noble metals (Au, Ag) are core layer for the nanocomposites and further confirm the formation of core-shell structure. Figure 4B shows the XPS spectra for the Y (3d) and Tb (4d) of Au@$NaYF_4$:Tb^{3+} and Ag@$NaYF_4$:Tb^{3+} and the curves fitted with a nonlinear least squares fitting program. The Y (3d) spectra show two strong peaks at 161.3 eV and 158.2 eV corresponding to $3d_{3/2}$ and $3d_{5/2}$, respectively. The relatively weak peak at around 152 eV can be assigned to the binding energy of
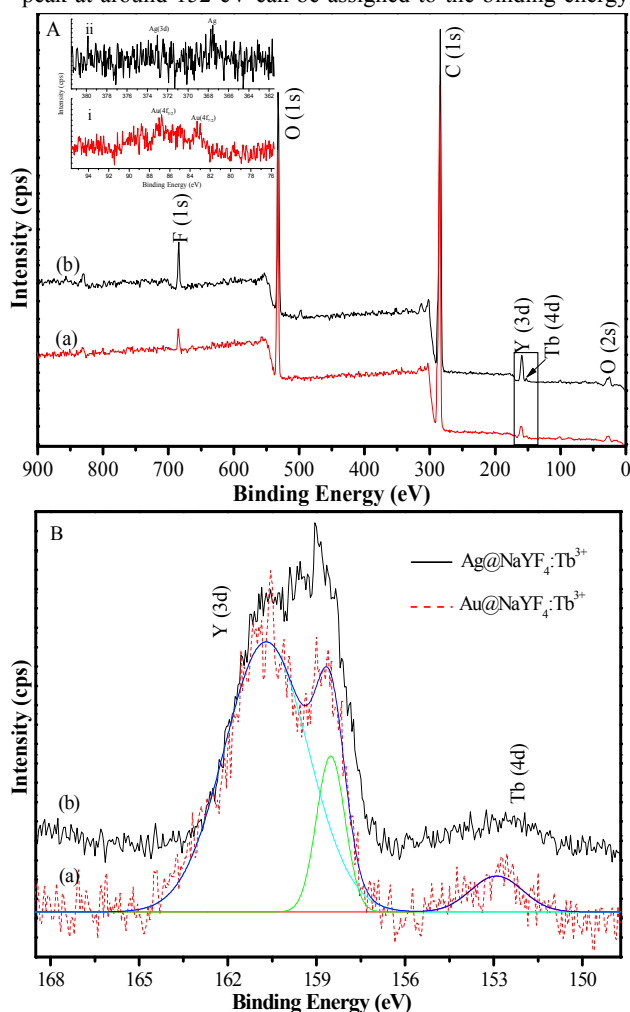
Figure 4. XPS spectra of (A) the wide range of Au@$NaYF_4$:Tb^{3+}(a) and Ag@$NaYF_4$:Tb^{3+}(b) , (B) Y (3d) and Tb (4d) spectra ofAu@$NaYF_4$:Tb^{3+} (a) and Ag@$NaYF_4$:Tb^{3+}(b). Inset shows the enlarged area corresponded to the Au (i) and Ag (ii) element.

Tb (4d) (Figure 4B). The low intensity of the photoelectron of Tb^{3+} is consistent with the relatively low doping concentration. The X-ray photoelectron spectra provides additional evidence for indicating that $NaYF_4$:Tb^{3+} have been successfully assembled on the surface of the metal nanoparticles.

3.3 Photoluminescence properties of core-shell structures

In order to investigate the energy transfer in core-shell hybrid nanoparticles, we compared the optical property of the $NaYF_4$:Tb^{3+} nanoparticles with Au@$NaYF_4$:Tb^{3+} nanoparticles. UV-Vis absorption spectroscopy experiments were carried out to confirm the plasmon absorption of gold nanoparticles. From Figure 5, the band observed at 520 nm is ascribed to the SPR absorption of gold nanoparticles. In view of that the ranges of spectra overlap between the emissions of $NaYF_4$:Tb^{3+} and the absorbance of Au nanoparticles is from 450 to 600 nm, we select the PL wavelength range from 400 to 700 nm (Figure 5), under excitation at 212 nm. The plasmonic absorption peaks of gold nanoparticles (520 nm) show considerable spectral overlap with the emission peaks of the $NaYF_4$:Tb^{3+} (544 nm) (Figure 5), indicating that energy transfer between $NaYF_4$:Tb^{3+} and Au nanoparticles is possible. For the $NaYF_4$:Tb^{3+}, the characteristic emissions centered at 451 nm, 454 nm, 485 nm, 544 nm, 586 nm and 621 nm are observed, which are assigned to the radiation transition of $^5D_3 \rightarrow {}^7F_J$ (J = 3,2) and $^5D_4 \rightarrow {}^7F_J$ (J = 6, 5, 4, 3) of Tb^{3+}, respectively. Among them, the peak at 544 nm is the strongest, and so the Au@$NaYF_4$:Tb nanoparticles do. In addition, the emission intensities of the $^5D_4 \rightarrow {}^7F_5$ and $^5D_4 \rightarrow {}^7F_6$ transition for the core-shell hybrid nanoparticles are attenuated clearly in the presence of a gold core. The emission intensity of $^5D_4 \rightarrow {}^7F_5$ transition is reduced more than of $^5D_4 \rightarrow {}^7F_6$. The fluorescent quenching can be attributed to the LRET between the Tb^{3+} emission bands and the gold plasmonic band.
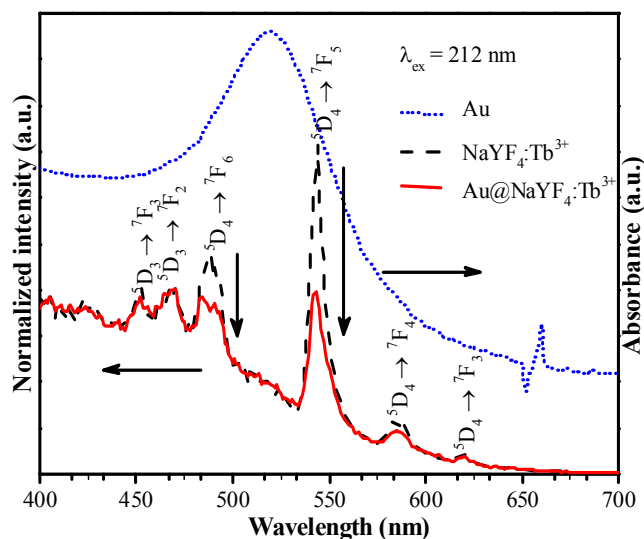
Figure 5. UV−Vis spectra of Au nanoparticles (dot), emission spectra of Au@$NaYF_4$:Tb^{3+} nanoparticles (solid) and $NaYF_4$:Tb^{3+} nanocrystals (dash)

The plasmonic absorption peak of silver nanoparticles is different from gold nanoparticles. The UV-Vis absorption band at 445 nm is observed in Figure 6, which is attributed to the SPR of

silver. Moreover, the range of absorption wavelength of silver nanoparticles is from 350 to 600 nm. For the emission spectra of Ag@NaYF$_4$:Tb^{3+}, the characteristic emissions peaks at 451 nm, 454 nm are not observed, which are assigned to the radiation transition of $^5D_3 \rightarrow {}^7F_J$ (J = 3,2) of Tb^{3+} compared with NaYF$_4$:Tb^{3+}. The emission intensity of the $^5D_4 \rightarrow {}^7F_5$ transition for the hybrid nanoparticles is attenuated clearly in the presence of a silver core and the emission intensity of $^5D_4 \rightarrow {}^7F_6$ transition is more significant reduced. Due to the greater overlap between the emission bands of $^5D_4 \rightarrow {}^7F_J$ (J= 6,5) transition and the plasmonic bands, greater intensity reduce for $^5D_4 \rightarrow {}^7F_6$ and $^5D_4 \rightarrow {}^7F_5$ transition in this case. This implies that spectral overlap is greater used for energy transfer from the luminescences nanoparticles to the noble metal nanoparticles. It is known that the efficiency of energy transfer is highly dependent on the extent of spectral overlap. The range of spectral overlap between the Tb^{3+} emission bands and the gold or silver plasmonic bands is different. The extent of emission intensity for Au@NaYF$_4$:Tb^{3+} is different from Ag@NaYF$_4$:Tb^{3+}.
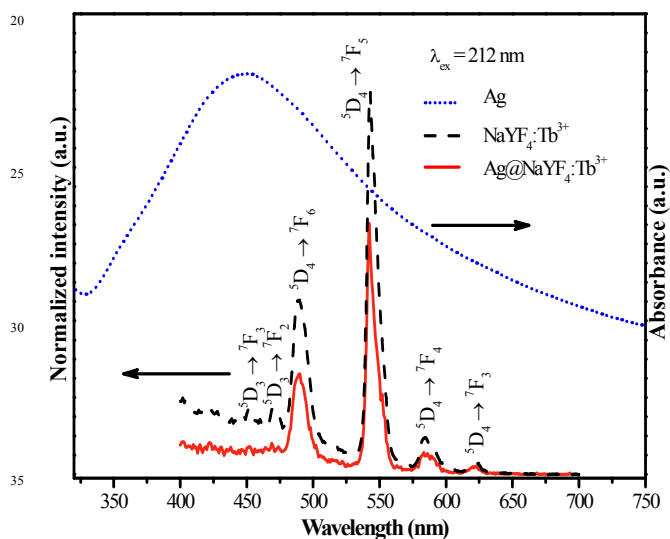
Figure 6. UV−Vis spectra of Ag nanoparticles (dot), emission spectra of Ag@NaYF$_4$:Tb^{3+} nanoparticles (solid) and NaYF$_4$:Tb^{3+} nanocrystals (dash)

In our case, the LRET system is formed by Au/Ag nanoparticles and NaYF$_4$:Tb^{3+} luminescent materials. In this LRET system, the NaYF$_4$:Tb^{3+} nanoshells serve as the energy donor and the Au/Ag nanoparticle cores are the energy receptor. As expected, the luminescence of the NaYF$_4$:Tb^{3+} nanocrystals is obviously quenched by Au/Ag nanoparticles via energy transfer from the NaYF$_4$:Tb^{3+} nanocrystals to noble metal nanoparticles for the spectral overlap between the emission of Tb^{3+} and the plasmonic absorption of noble metals.

To further clarify this effect, the luminescence decay curves for the $^5D_4 \rightarrow {}^7F_6$ and $^5D_4 \rightarrow {}^7F_5$ transition of Tb^{3+} ions in NaYF$_4$:Tb^{3+}, Au@NaYF$_4$:Tb^{3+} and Ag@NaYF$_4$:Tb^{3+} nanoparticles were measured at room temperature, respectively. Figure 7 shows the normalized decay profiles of the $^5D_4 \rightarrow {}^7F_6$ and $^5D_4 \rightarrow {}^7F_5$ transition at 489 nm and 544 nm, respectively. Both decay curves can be fitted well with a single exponential function of I=I$_0$+Aexp(-x/τ) (τ corresponds to the lifetime of Tb^{3+}). As shown in Figure 7, the

lifetimes of the $^5D_4 \rightarrow {}^7F_6$ and $^5D_4 \rightarrow {}^7F_5$ transitions of Tb^{3+} are decreased in the presence of Au and Ag core. It can be observed that there is a clear decrease in the emission lifetime of $^5D_4 \rightarrow {}^7F_6$ of Tb^{3+} in NaYF$_4$:Tb^{3+} which varies from 10.16 ms to 8.46 ms and 7.26 ms in the absence and presence of gold and silver nanoparticles, respectively (Figure 7 A). The lifetime of Tb^{3+} in Au@NaYF$_4$Tb^{3+} is longer than that of in Ag@NaYF$_4$:Tb^{3+}. Whereas the emission lifetime of $^5D_4 \rightarrow {}^7F_5$ of Tb^{3+} in NaYF$_4$:Tb^{3+} varies from 7.54 ms to 6.20 ms and 7.18 ms in the absence and presence of gold and silver nanoparticles (Figure 7 B). The lifetime of Tb^{3+} ($^5D_4 \rightarrow {}^7F_5$) in Au@NaYF$_4$:Tb^{3+} is shorter than that of in Ag@NaYF$_4$:Tb^{3+}. Therefore, it supplies direct proof for the conclusion that the energy transfer from NaYF$_4$:Tb^{3+} nanocrystals to gold or silver nanoparticles is different, which depends on the range of spectral overlap. This efficient energy transfer can be provided more energy for gold nanoparticles, which will be used for scatter light and plasmonic absorption. The results show that the LRET system based on the lanthanide doped luminescent materials and noble metal nanoparticles is very efficient and versatile. Applications of the LRET system in fluorescence immunoassays, DNA detection, and fluorescence imaging are in progress.
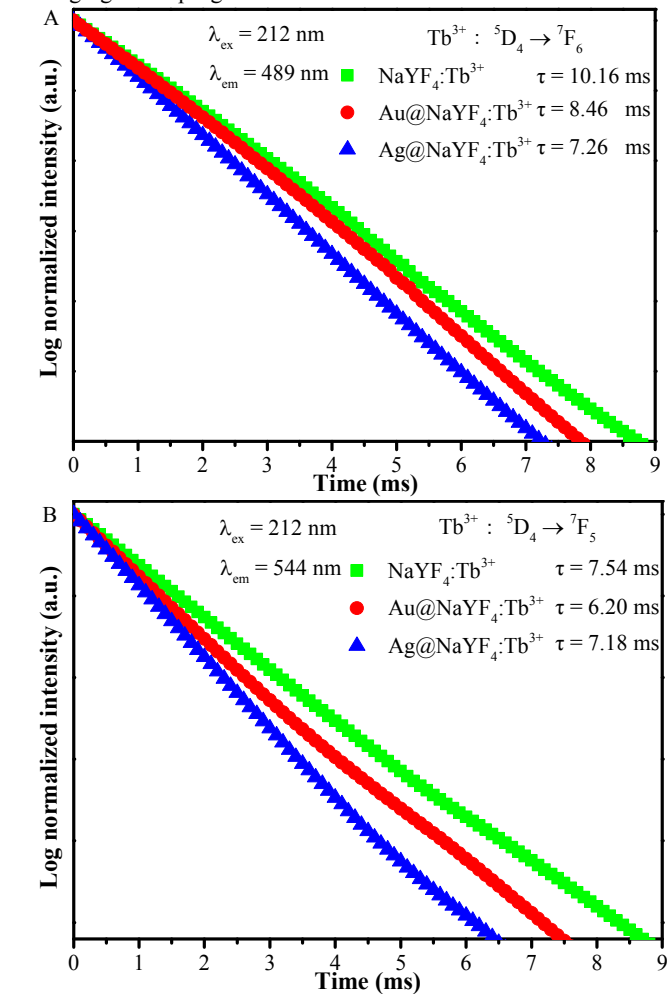
Figure 7. Luminescence decay curves of Tb^{3+} $^5D_4 \rightarrow {}^7F_6$ (A) and $^5D_4 \rightarrow {}^7F_5$ (B) transitions, in NaYF$_4$:Tb^{3+} (a), Au@NaYF$_4$:Tb^{3+} (b) and Ag@NaYF$_4$:Tb^{3+} nanoparticles (c).
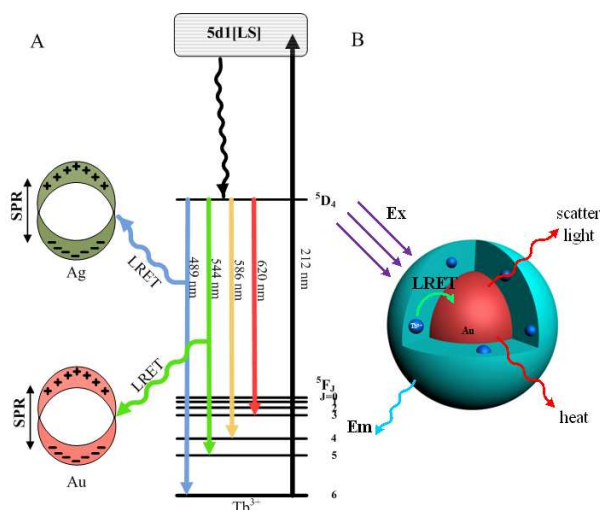
Figure 8. (A) Energy level diagram of Tb^{3+} and (B) schematic illustration of the LRET process, with $NaYF_4$:Tb^{3+} nanocrystals as energy donors and Au nanoparticles as energy acceptors.

According to the theory of LRET, when the donor and the acceptor are physically close together and possess the amount of spectral overlap, the emission of the energy donor is quenched by the energy acceptor and at the same time, the resonance energy transfer is occurred. In our work, the LRET system can be constructed as shown in Figure 8, combining $NaYF_4$:Tb^{3+} nanocrystals and gold nanoparticles served as energy donor and acceptor, respectively. When gold nanoparticles are introduced into the nanocomposites, the energy transfer from $NaYF_4$:Tb^{3+} nanocrystals to gold nanoparticles occurs in the LRET systems owning to the absorption spectrum of Ag and Au nanoparticles matches well with the emission band of Tb^{3+} at 489 nm and 544 nm, respectively. Figure 8 A shows that the emissive energy transferred by LRET from $^5D_4 \rightarrow ^7F_6$(489 nm) and $^5D_4 \rightarrow ^7F_5$(544 nm) transition of Tb^{3+} to Ag and Au. The results establish that there exists an energy transfer from Tb^{3+} ions to noble metal nanoparticles and the resonant excitation is ruled out. In the Au@$NaYF_4$:Tb^{3+} nanocomposites, the donor fluorescence decreases or quenches because of energy transfer and a reduction of excited state lifetime accompanied by the means of increasing non-radiative decay rate and decreasing radiative rate of the $NaYF_4$:Tb^{3+} nanocrystals. Gold nanoparticles as energy acceptor will convert energy to heat and produce stronger scatter light. The scatter light and heat will greatly be useful in biological imaging and photothermal therapy.

4 Conclusions

In summary, we have synthesized the Au@$NaYF_4$:Tb^{3+} and Ag@$NaYF_4$:Tb^{3+} core-shell nanoparticles with good crystallinity, strong fluorescence and controllable size. The synthetic methodology also can be used to prepare other single-emission lanthanide luminescent nanoparticles. We have developed a LRET system using promising lanthanide-doped nanoparticles to serve as energy donor and noble metal nanoparticles as energy acceptor. It is interesting to observe that the plasmonic absorption bands of gold or silver nanoparticles show considerable spectral overlap with the emission bands of $^5D_4 \rightarrow ^7F_j$ (j= 6,5) transition of

Tb^{3+} in the $NaYF_4$:Tb^{3+}. The greater spectral overlap leads to highly efficient LRET. We observe that the emission intensity of the $NaYF_4$:Tb^{3+} nanocrystals is significantly quenched in the presence of gold and silver nanoparticles. The effect can be attributed primarily to the plasmon resonance absorption by gold and silver nanoparticles. The photoluminescence decay time measurements show that the $NaYF_4$:Tb^{3+} nanocrystals exhibit long PL lifetime and slightly decreased as a result of interaction with the noble metal nanoparticles. The analysis results suggest the possibility of energy transfer from the $NaYF_4$:Tb^{3+} nanocrystals to gold or silver nanoparticles. We envision that the core-shell hybrid nanoparticles based on the lanthanide and noble metal will offer potential application in the biomedical fields, including multimodal imaging in vitro or in vivo and photothermal therapy of cancer.

Acknowledgment

Notes and references

Key Laboratory of Applied Chemistry and Nanotechnology at Universities of Jilin Province, Changchun University of Science and Technology, Changchun 130022, P. R. China. Tel.:+86-431-85582574. Fax.: +86-431-85383815; E-mail address: liuguixia22@163.com

1   M. Rycenga, C. M. Cobley, J. Zeng, W. Li, C. H. Moran, Q. Zhang, D. Qin and Y. Xia, *Chem. Rev.,* 2011, **111**, 3669-3712.
2   S. K. Ghosh and T. Pal, *Chem. Rev.,* 2007, **107**, 4797-4862.
3   K. E. Fong and L. Y. Yung, *Nanoscale*, 2013, **5**, 12043-12071.
4   V. W. K. Ng, R. Berti, F. e. e. Lesage and A. Kakkar, *J. Mater. Chem. B*, 2013, **1**, 9-25.
5   Y. Wang, Y. Liu, H. Luehmann, X. Xia, D. Wan, C. Cutler and Y. Xia, *Nano Lett.,* 2013, **13**, 581-585.
6   S. F. Lai, C. C. Chien, W. C. Chen, H. H. Chen, Y. Y. Chen, C. L. Wang, Y. Hwu, C. S. Yang, C. Y. Chen, K. S. Liang, C. Petibois, H. R. Tan, E. S. Tok and G. Margaritondo, *Biotechnol. Adv.* 2013, **31**, 362-368.
7   A. J. Mieszawska, W. J. Mulder, Z. A. Fayad and D. P. Cormode, *Mol. pharm.,* 2013, **10**, 831-847.
8   E. Boisselier and D. Astruc, *Chem. Rev.,* 2009, **38**, 1759-1782.
9   E. C. Dreaden, A. M. Alkilany, X. Huang, C. J. Murphy and M. A. El-Sayed, *Chem. Soc. Rev.,* 2012, **41**, 2740-2779.
10 R. R. Arvizo, S. Bhattacharyya, R. A. Kudgus, K. Giri, R. Bhattacharya and P. Mukherjee, *Chem. Soc. Rev.,* 2012, **41**, 2943-2970.
11 L. Dykman and N. Khlebtsov, *Chem. Soc. Rev.,* 2012, **41**, 2256-2282.
12 W. Ge, X. R. Zhang, M. Liu, Z. W. Lei, R. J. Knize and Y. Lu, *Theranostics*, 2013, **3**, 282-288.
13 P. Reineck, D. Gómez, S. H. Ng, M. Karg, T. Bell, P. Mulvaney and U. Bach, *ACS Nano*, 2013, **7**, 6636-6648.
14 O. Kulakovich, N. Strekal, A. Yaroshevich, S. Maskevich, S. Gaponenko, I. Nabiev, U. Woggon and M. Artemyev, *Nano Lett.*, 2002, **2**, 1449-1452.
15 J. Yang, F. Zhang, Y. Chen, S. Qian, P. Hu, W. Li, Y. Deng, Y. Fang, L. Han, M. Luqman and D. Zhao, *Chem. Commun.*, 2011, **47**, 11618-11620.
16 D. Darvill, A. Centeno and F. Xie, *Phys. Chem. Chem. Phys.*, 2013, **15**, 15709-15726.
17 F. Zhang, G. B. Braun, Y. Shi, Y. Zhang, X. Sun, N. O. Reich, D. Zhao and G. Stucky, *J. Am. Chem. Soc.*, 2010, **132**, 2850-2851.
18 P. Yuan, Y. H. Lee, M. K. Gnanasammandhan, Z. Guan, Y. Zhang and Q. H. Xu, *Nanoscale*, 2012, **4**, 5132-5137.
19 W. Xu, S. Xu, Y. Zhu, T. Liu, X. Bai, B. Dong, L. Xu and H. Song,

Nanoscale, 2012, **4**, 6971-6973.

20 L. Sudheendra, V. Ortalan, S. Dey, N. D. Browning and I. M. Kennedy, *Chem. Mater.,* 2011, **23**, 2987-2993.

21 C. Zhang and J. Y. Lee, *J. Phys. Chem. C,* 2013, **117**, 15253-15259.

22 A. Priyam, N. M. Idris and Y. Zhang, *J. Mater. Chem.,*2012, **22**, 960-965.

23 G. Chen, F. Song, X. Xiong and X. Peng, *Ind. Eng. Chem. Res.*, 2013, **52**, 11228-11245.

24 M. Ray, T. S. Basu, N. R. Bandyopadhyay, R. F. Klie, S. Ghosh, S. O. Raja and A. K. Dasgupta, *Nanoscale*, 2014, **6**, 2201-2210.

25 W.-W. Zhao, J. Wang, J.-J. Xu and H.-Y. Chen, *Chem. Commun.*, 2011, **47**, 10990-10992.

26 H. Sun, J. He, J. Wang, S.-Y. Zhang, C. Liu, T. Sritharan, S. Mhaisalkar, M.-Y. Han, D. Wang and H. Chen, *J. Am. Chem. Soc.*, 2013, **135**, 9099-9110.

27 A. D. Quach, G. Crivat, M. A. Tarr and Z. Rosenzweig, *J. Am. Chem. Soc.*, 2011, **133**, 2028-2030.

28 S. Raut, R. Rich, R. Fudala, S. Butler, R. Kokate, Z. Gryczynski, R. Luchowski and I. Gryczynski, *Nanoscale*, 2014, **6**, 385-391.

29 Y. Liu, D. Tu, H. Zhu and X. Chen, *Chem. Soc. Rev.*, 2013, **42**, 6924-6958.

30 L. Wang, R. Yan, Z. Huo, L. Wang, J. Zeng, J. Bao, X. Wang, Q. Peng and Y. Li, *Angew. Chem. Int. Ed.*, 2005, **44**, 6054-6057.

31 J. Q. Gu, L. D. Sun, Z. G. Yan and C. H. Yan, *Chem.-Asian J*, 2008, **3**, 1857-1864.

32 M. Wang, W. Hou, C.-C. Mi, W.-X. Wang, Z.-R. Xu, H.-H. Teng, C.-B. Mao and S.-K. Xu, *Anal. Chem.*, 2009, **81**, 8783-8789.

33 D. Tu, L. Liu, Q. Ju, Y. Liu, H. Zhu, R. Li and X. Chen, *Angew. Chem. Int. Ed.*, 2011, **50**, 6306-6310.

34 H. Q. Chen, F. Yuan, S. Z. Wang, J. Xu, Y. Y. Zhang and L. Wang, *Analyst*, 2013, **138**, 2392-2397.

35 C. Mi, H. Gao, F. Li and S. Xu, *Colloids Surf., A*, 2012, **395**, 152-156.

36 Z. Wang, L. Wu, B. Shen and Z. Jiang, *Talanta*, 2013, **114**, 124-130.

37 A. Podhorodecki, M. Banski, A. Noculak, B. Sojka, G. Pawlik and J. Misiewicz, *Nanoscale*, 2013, **5**, 429-436.

38 G Frens. Nature, 1973, **241**: 20-22.

39 B V Enustun and J Turkevich. *J. Am. Chem. Soc.*, 1963, **85**, 3317-3328.